Vol. 48 — N° 1 03 24 p. 227 – 244

GEOSTANDARDS and GEOANALYTICAL RESEARCH

New Potential Sulfide Reference Materials for Microbeam S-Fe-Cu Isotope Measurements

Yantong **Feng** (1, 2), Wen **Zhang** (2)*, Zhaochu **Hu** (2), Tao **Luo** (2), Qinglin **Li** (2) and Jinyu **Liu** (2)

(1) Gansu Key Laboratory of Mineral Resources in Western China, School of Earth Sciences, Lanzhou University, Lanzhou 730000, China
(2) State Key Laboratory of Geological Processes and Mineral Resources, China University of Geosciences, Wuhan 430074, China
* Corresponding author. e-mail: tuyaken@hotmail.com

S-Fe-Cu isotope systems are powerful tracers for revealing geochemical processes. However, the microanalysis of S-Fe-Cu isotopes is critically limited by the lack of suitable reference materials. Herein, we present three potential reference materials Ll-Cpy (chalcopyrite), Ll-Po (pyrrhotite) and Ll-Sp (sphalerite) for *in situ* S-Fe-Cu isotope measurements. Numerous *in situ* S-Fe-Cu isotope measurements were performed over two years to assess isotopic homogeneity. The bulk S isotopic compositions were determined independently in seven laboratories by isotope ratio mass spectrometry (IRMS); the preferred $\delta^{34}S_{V\text{-}CDT}$ for Ll-Cpy, Ll-Po, Ll-Sp are 6.13 ± 0.37‰ (2*s*), 6.42 ± 0.37‰ (2*s*) and 6.28 ± 0.38‰ (2*s*), respectively. The bulk Fe isotope ratios in Fe-bearing Ll-Cpy and Ll-Po were determined using solution nebulisation multi-collector inductively coupled plasma-mass spectrometry, and the obtained $\delta^{56}Fe_{IRMM\text{-}014}$ values are 0.57 ± 0.07‰ (2*s*) and -0.62 ± 0.07‰ (2*s*), respectively. The mean bulk $\delta^{65}Cu_{NIST\ SRM\ 976}$ value of Ll-Cpy is 0.57 ± 0.06‰ (2*s*). All the bulk values are in good agreement with the long-term statistical results of laser ablation-MC-ICP-MS and proposed as the recommended values. These sulfides are well characterised and isotopically homogeneous (at 30–40 μm spatial resolution), and can be used as potential calibration materials for *in situ* S-Fe-Cu isotope measurements.

Keywords: chalcopyrite, pyrrhotite, sphalerite, reference materials, S-Fe-Cu isotopes, LA-MC-ICP-MS.

Received 22 May 23 – Accepted 19 Sep 23

Sulfur (S), iron (Fe) and copper (Cu) are ubiquitous elements with different oxidation states that are heterogeneously distributed throughout reservoirs (Sawaki *et al.* 2018, Paiste *et al.* 2022, Smith *et al.* 2022, McLoughlin *et al.* 2023). The S-Fe-Cu isotope systems in sulfides have been well proven to be excellent geochemical tracers in diverse fields of geoscience, such as research on planetary evolution events, mineralisation mechanisms, hydrothermal activity and bioenvironmental processes (Li *et al.* 2010, Marin-Carbonne *et al.* 2014, Mount *et al.* 2022, Hiebert *et al.* 2016, Brzozowski *et al.* 2021, Yu *et al.* 2021, Lehmann *et al.* 2022, Zhao *et al.* 2022).

In general, S isotopes are measured by gas-source isotope ratio mass spectrometry (GS-IRMS) (Ke *et al.* 2017), whereas Fe and Cu isotope ratios are usually determined by solution nebulisation multi-collector ICP-MS (SN-MC-ICP-MS) after complex whole-rock dissolution and chemical purification processes (Sossi *et al.* 2015, Zhu *et al.* 2019). These bulk analytical techniques are considered the standard methods for isotope ratio determinations; however, chemical pretreatment is time-consuming and requires large amounts of reagents (Baublys *et al.* 2004, Zhu et al. 2019, Lei *et al.* 2022). In particular, avoiding contamination from inclusions or to distinguishing the information from the small mineral scale is difficult. Thus, an *in situ* analytical approach for S-Fe-Cu isotopic analysis is needed to meet the demands of numerous applications (Jenner and Arevalo 2016, Müller and Fietzke 2016).

In the last two decades, microanalytical techniques such as secondary ion mass spectroscopy (SIMS) and laser ablation (LA)-MC-ICP-MS have been widely used and have considerably advanced isotope geochemistry research (Resano *et al.* 2013, Oeser *et al.* 2015, Zheng *et al.* 2017, Hammerli *et al.* 2021, Hu *et al.* 2022). However, the

doi: 10.1111/ggr.12530

matrix effect remains an intractable problem that impedes the development of these *in situ* techniques for S-Fe-Cu isotope measurement (Gilbert *et al.* 2014, Lazarov and Horn 2015, Wohlgemuth-Ueberwasser and Jochum 2015). The use of matrix-matched reference materials is considered the simplest and most effective approach to overcome the matrix effect (Wilson *et al.* 2002, Jackson *et al.* 2003, Nasdala *et al.* 2018, Hu *et al.* 2021, Luo *et al.* 2021).

Recently, an increasing number of studies have focused on developing sulfide reference materials (LaFlamme *et al.* 2016, Onuk *et al.* 2017, Chen *et al.* 2021a). Natural minerals are the best choice among all reference materials because complete matrix matching (chemical composition and physical properties) can be achieved during microanalysis. Although considerable effort has been focused on preparing S-Fe-Cu isotope reference materials, to the best of our knowledge most of these reference materials are only for the determination of one of the S-Fe-Cu isotopes, and certain substances are almost exhausted or are no longer available (Tables 1–3).

In this paper, we present natural chalcopyrite, pyrrhotite and sphalerite candidate reference materials for *in situ* S-Fe-Cu isotope measurement. Numerous LA-MC-ICP-MS measurements and bulk analyses were performed to assess the S-Fe-Cu isotope ratios of these samples. The results show that these sulfides are well characterised and isotopically homogeneous and can be used as reference materials for *in situ* S-Fe-Cu isotope measurements. These reference materials are available in sufficient amounts to be shared with other *in situ* analytical laboratories.

Sample description and preparation

The sulfide samples (Figure 1a-c) in this study were collected from the Linglong golden deposit located in the Jiaodong area in the eastern part of the North China Craton. The deposit is one of the largest quartz vein-type gold deposits in Jiaodong, where the ore formation is mainly controlled by a NNE-NE trending fault zone. Here, the masses of these three massive sulfides are ~ 6.4 (Figure 1a), ~ 0.7 (Figure 1b) and ~ 1.0 kg (Figure 1c).

The massive sulfide samples (Figure 1a–c) comprise 80% chalcopyrite, 10% pyrrhotite, 5% sphalerite and minor amounts of mica and quartz. One-tenth of the three massive sulfide samples (total mass ~ 800 g) were selected for mineral separation, yielding ~ 500 g pure chalcopyrite

Table 1.
Recent studies on natural sulfide reference materials (RMs) for *in situ* sulfur isotope measurement

Mineral	RM name	δ^{34}S (‰)	2*s*	Instrument	Sample amount	Collection site	Reference
Pyrite	PPP-1	5.3	0.2	Ion microprobe and IRMS	Massive mineral specimens	Recrystallised sedimentary pyrite, Sukhoi Log deposit, Russia	Gilbert *et al.* (2014)
Pyrrhotite	Po-10	6	0.3				
Bornite	N-11	-4.4	0.6				
Pyrite	Sierra	2.17	0.25	SIMS	A 2 cm^3 cube	Cretaceous stratigraphy mine of Mexico	LaFlamme *et al.* (2016)
Chalcopyrite	Nifty-b	-3.58	0.23		A 2 cm^3 piece of a larger 8 cm^3 grain	Copper deposit in Western Australia	
Pyrrhotite	Alexo	5.23	0.30		0.1–2 mm grains	Alexo Ni-Cu-(PGE) deposit in Canada	
Pentlandite	VMSO	3.22	0.33		0.1–0.5 mm magmatic pentlandite grains	Sulfide deposits in Western Australia	
Chalcopyrite	Cpy-1	4.21	0.23	LA-MC-ICP-MS	Mineral aggregation	-	Chen *et al.* (2017)
	GC	-0.70	0.2				
Pyrrhotite	YP136	1.5	0.3	SIMS	Drill core	Mafic complex in northern Finland	Li *et al.* (2018)
Chalcopyrite	HTS4-6	0.58	0.39	SIMS/LA-MC-ICP-MS	Total of 102 g	Sulfide deposit located in Liaoning, China	Li *et al.* (2020)
Pyrrhotite	Jc-Po	0.06	0.27	SIMS	Hand specimen, and handpicked ~ 8 g of pyrrhotite grains and 3 g of pentlandite	Jinchuan Ni-Cu-PGE sulfide deposit, south-western China	Chen *et al.* (2021b)
Pentlandite	Jc-Pn	-0.09	0.19				
Chalcopyrite	TC1725	12.78	0.38	LA-MC-ICP-MS	The hand specimen prepared to four strips and five epoxy mounts	Tongchang copper deposit, Jiangxi, China	Bao *et al.* (2021b)
Galena	NWU-GN	28.21	0.17	LA-MC-ICP-MS	~ 100 g of galena fragments	Changbei Pb-Zn deposit, Gansu, China	Lv *et al.* (2022)
Chalcopyrite	GC-1	-0.65	0.28		~ 40 g	Guichi copper mine in Anhui, China.	
Sphalerite	SPH-1	-7.13	0.41		Total mass of 40 g	Kangjiawan Pb-Zn sulfide deposit, Hunan, China	

Table 2.
Recent studies on natural sulfide RMs for *in situ* iron isotope measurement

Minerals	RM Name	δ^{56}Fe (‰)	2*s*	Instrument	Sample amount	Collection site	Reference
Pyrrhotite	Jc-Po	-0.34	0.33	LA-MC-ICP-MS	Hand specimen, and handpicked ~ 8 g of pyrrhotite grains and 3 g of pentlandite	Jinchuan Ni-Cu-PGE sulfide deposit, southwestern China	Chen *et al.* (2021b)
Pentlandite	Jc-Pn	1.47	0.46				
Pyrite	Py1308	0.36	0.28		20 g, 10 × 8 × 5 mm cubic crystal	Guangdong, China	Chen *et al.* (2021a)
	CB	-0.89	0.07		5 g, 200–400 μm idiomorphic granular	Changba Pb-Zn deposit, Gansu, China	
	Aa018	0.52	0.10		37 g, 15 × 15 × 10 mm cubic crystal	Navarra, Spain	
	LY	0.60	0.08		80 g, 26 × 18 × 34 mm cubic crystal	Liyang, Hunan, China	
	Py-Bal-13B	-1.38	0.11		-	-	
Chalcopyrite	Ccp2656	0.10	0.12		-	-	
Pyrite	Balmat	-1.27	0.12		-	Balmat deposit, USA	Xu *et al.* (2022)
Pyrite	NKAu01	0.35	0.15		~ 1.3 kg, 6.5 × 6.5 × 6.5 cm	Mofang gold deposit, North Korea	
Pyrite	Tianyu-Py	0.49	0.20		Handpicked ~ 4 g of pure pyrite grains	Tianyu magmatic sulfide deposit, China	Chen *et al.* (2022a, 2023)
Chalcopyrite	Tianyu-Ccp	0.39	0.19		~ 20 g of the pure chalcopyrite grains		

Table 3.
Recent studies on natural sulfide RMs for *in situ* copper isotope measurement

Mineral	RM name	δ^{65}Cu (‰)	2*s*	Instrument	Sample amount	Collection site	Reference
Chalcopyrite	Bougainlille	-0.81	0.06	LA-MC-ICP-MS	-	Bougainville porphyry copper deposit, Papua New Guinea	Li *et al.* (2010)
	TC1725	-1.27	0.04		Hand specimen prepared to four strips and five epoxy mounts	The Tongchang copper deposit, China	Bao *et al.* (2021a)
	14ZJ12-1	-0.21	0.07		Mineral grains, 150 g	Xiaseling Cu-W deposit, China	Yang *et al.* (2023)
	JGZ-22	0.46	0.08		Mineral grains, 100 g	Jiguanzui Cu-Au deposit, China	
	JGZ-78	-0.06	0.08		Mineral grains, 80 g		
	TQ-Ccp	0.04	0.04		Fragments, > 50 g	Tianqiao Pb-Zn deposit, China	Fang *et al.* (2023)

The δ values of S-Fe-Cu isotopes are all given by the bulk analysis method. 2*s* is the uncertainty of sample uniformity obtained by *in situ* measurements.

(Ll-Cpy), ~ 40 g pure pyrrhotite (Ll-Po), and ~ 20 g pure sphalerite (Ll-Sp) fragments, respectively. Then, approximately 10 g of pure Ll-Cpy and Ll-Po fragments were selected and packed into 100 tubes (numbered 1–100), whereas 0.8 g of pure Ll-Sp fragments were packed into eight tubes (numbered as 1–8) as distributable samples (Figure 2). Ll-Cpy and Ll-Po tubes were numbered in multiples of ten, and furthermore all Ll-Sp tubes were selected for the preparation of epoxy resin mounts (~ 200 fragments for each mount). The remaining pure mineral segments were stored for distribution and reselection. The remaining massive sulfide samples were not separated to avoid oxidation.

Analytical methods

Electron probe microanalysis (EPMA), LA-(MC)-ICP-MS, IRMS and SN-MC-ICP-MS were employed to determine the chemical and isotope compositions of the candidate sulfide reference materials.

First, EPMA and LA-ICP-MS were used to measure the chemical composition of each candidate reference material. Backscattered electron images were used to highlight potential chemical zonation, mineralogical inclusions and fractures in the candidate reference materials. Second, LA-MC-ICP-MS was used to determine isotope ratios in each candidate reference material. Isotopic homogeneity was assessed by the reproducibility of the candidate material. Finally, IRMS and SN-MC-ICP-MS were used to determine the bulk S and Fe-Cu isotopic compositions, respectively. Details of the analytical techniques and processes are described below.

EPMA and LA-ICP-MS

Elemental mass fractions were measured using EPMA and LA-ICP-MS. The EPMA measurements were performed at the Wuhan Sample Solution Analytical Technology Co. Ltd., Wuhan, China. The analytical conditions of the JEOL

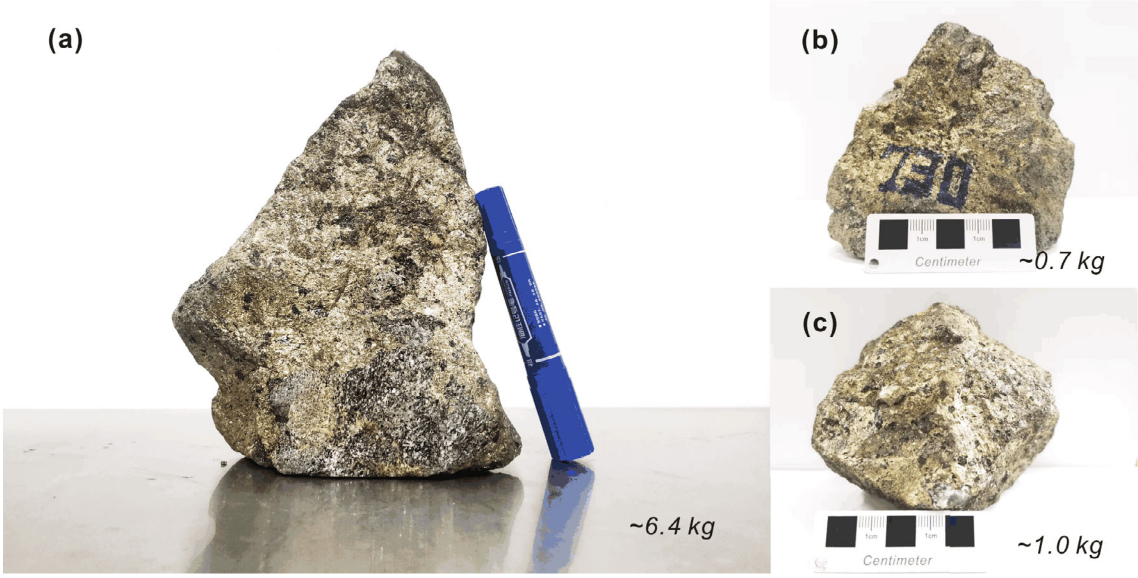

Figure 1. Photographs of the collected massive sulfide samples.

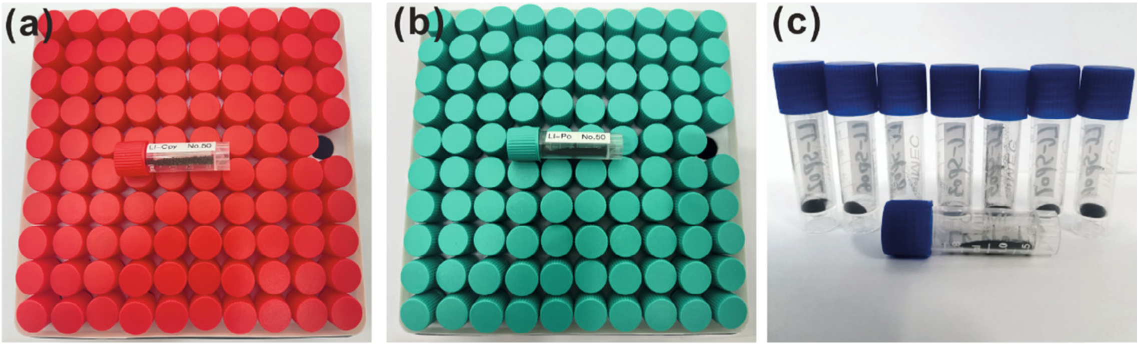

Figure 2. Photographs of sub-packages of (a) Ll-Cpy, (b) Ll-Po and (c) Ll-Sp minerals. Each tube is filled with approximately 100 mg of pure sample grains. A total of 100 tubes for both Ll-Cpy and Ll-Po (numbered 1–100), and eight tubes for Ll-Sp (numbered 1–8).

JXA-8230 electron probe employed for all elements included an accelerating voltage of ~ 20 kV, a beam current of 50 nA and a beam size of 1 μm. In addition, several critical trace elements were determined (such as Cr, which had an isobaric interference of ^{54}Cr on ^{54}Fe) in Ll-Cpy and Ll-Po fragments by LA-ICP-MS to assess interferences during isotope measurement. LA-ICP-MS experiments were performed at the State Key Laboratory of Geological Processes and Mineral Resources (GPMR), China University of Geosciences, Wuhan. An Agilent 7900 quadruple ICP-MS instrument (Agilent Technology, Tokyo, Japan) combined with a GeoLas HD laser ablation system (Coherent Inc., Göttingen, Germany) was used for the quantitative analysis in this study. The details of the analytical method are described in Feng *et al.* (2018).

In situ S-Fe-Cu isotope measurements by (fs)-LA-MC-ICP-MS

The *in situ* isotopic measurements were conducted at the GPMR and the State Key Laboratory of Continental Dynamics (SKLCD), Northwest University. For S isotope measurement in GPMR, a NEPTUNE Plus MC-ICP-MS instrument (Thermo Fisher Scientific, Bremen, Germany) was combined with a NWR FemtoUC femtosecond system (New Wave Research, Fremont, CA, USA) for these experiments. The NEPTUNE Plus instrument was a double focusing MC-ICP-MS equipped with seven fixed electron multiplier ion counters and nine Faraday cups fitted with 10^{11} Ω resistors. In addition, a large dry interface pump (100 m^3 h^{-1} pumping speed), an X skimmer cone and a Jet sample cone were used for isotope measurements. The LA system consisted of a 300 fs Yb:KGW femtosecond laser amplifier (PHAROS, Light Conversion Ltd., Vilnius, Lithuania) with a wavelength of 257 nm, and was equipped with a two-volume cell, which had a constant distance between the laser ablation and aerosol extraction positions. Helium gas was used as the carrier gas, and a signal-smoothing device was used downstream of the sample cell to enhance the stability of the ablation signal (Hu *et al.* 2012). The single-spot ablation mode was used with a spot size of 40 μm, a repetition rate of 3 Hz and a laser fluence of ~ 3.5 J cm^{-2}. Signals of ^{32}S, ^{33}S and ^{34}S were collected in the L2, centre and H2 Faraday cups, respectively. Approximately 4 ml min^{-1} of nitrogen was added to the central gas flow to reduce polyatomic interferences (Fu *et al.* 2016). All measurements were performed in static mode using medium resolution with a resolving power of 4000. Individual data acquisition consisted of one block of 120 cycles with an integration time of 0.524 s per cycle. The total acquisition time for each measurement was approximately 63 s, including 15 s of background signal following a time of 40 s for ablation signal acquisition, and 8 s for wash-out. The mean background intensity was subtracted from each individual data sweep of the ablation signal for a given isotopic mass. The standard-sample-bracketing method (SSB) was employed to correct instrumental drift and mass bias. Pyrrhotite reference material YP136 was used as the calibrator, whereas the pyrite reference material PPP-1, chalcopyrite reference material HTS4-6 and sphalerite reference material SPH-1 were analysed in different measurement sessions as unknown samples to verify the accuracy of the calibration method. Details of the fs-LA-MC-ICP-MS operating conditions and measurement parameters are summarised in Table 4.

In general, sulfur isotope ratios are expressed in delta (δ) notation (per mill, ‰) as follows:

$$\delta^{x}S = \left[\left({}^{x}S/{}^{32}S\right)_{sample}/\left({}^{x}S/{}^{32}S\right)_{RM}\right] - 1 \qquad (1)$$

where "sample" and "RM" represent the measured samples and the reference material YP136, respectively, and x is the mass number 34.

Table 4.
The fs-LA-MC-ICP-MS operating parameters for S-Fe-Cu isotope measurements

Neptune Plus MC-ICP-MS	
RF Power	1200 W
Cool gas flow	16.0 l min^{-1}
Auxiliary gas flow	0.8–1.2 l min^{-1}
Argon make-up gas flow	0.6–1.0 l min^{-1}
Helium carrier gas flow	0.6–0.7 l min^{-1}
Interface cones	X skimmer cone + Jet sample cone
Block number	1
Integration time	0.524 s
Laser ablation system	
Laser type	Yb: KGW femtosecond laser
Wavelength	257 nm
Pulse width	300 fs
Energy density	~ 2.5–3.5 J cm^{-2}
Spot size	30–40 μm
Repetition rate	3 Hz

At the SKLCD, a 193 nm excimer LA system (RESOlution M-50, ASI) was coupled with a Nu 1700 MC-ICP-MS (Nu 1700, Nu Instruments, Wrexham, UK) for *in situ* S isotope ratio measurements. All measurements were carried out in single-spot ablation mode with spot sizes in the range 43–67 μm, while the signal intensity ranged from 10 to 15 V. Each sample acquisition consisted of 30 s background, 40 s data collection, and 50 s wash-out time measurements. The SSB protocol was used to calibrate the mass bias of the instrument. The details of the analytical procedure are described by Bao *et al.* (2021b), Chen *et al.* (2022b) and Lv *et al.* (2022). For the chalcopyrite S isotope measurements, Cpy1 and TC1725 (Bao *et al.* 2021b) were used as the calibration material and unknown sample. For pyrrhotite S isotope measurement, PY4 was used as the calibration material, whereas RPPY (Lv *et al.* 2022, Chen *et al.* 2022b) was used as the unknown sample.

For *in situ* Fe and Cu isotope measurements at GPMR, the single-spot ablation mode with a size of 30–40 μm, repetition rate of 3 Hz and a laser fluence of ~ 2.5–3.5 J cm^{-2} was also used. A small amount of ultra-pure water was introduced downstream of the ablation cell to create a "wet" plasma atmosphere in the ICP to suppress the matrix effect during measurement (Zheng *et al.* 2018, Chen *et al.* 2021a, Zhang *et al.* 2022). All measurements were performed in static mode while using low-resolution (resolving power of 400) for Cu isotope measurements and high resolution (resolving power of 7000) for Fe isotope measurements. Both the data acquisition and LA process were similar to those in the S isotope experiment. The SSB method was employed to correct instrumental drift and mass bias for Fe and Cu isotope measurements. The cup configurations for Fe isotope measurement were set to: L4 (^{53}Cr), L1 (^{54}Fe), C (^{56}Fe), H1 (^{57}Fe), H2 (^{58}Fe) and H4 (^{60}Ni). ^{53}Cr and ^{60}Ni were monitored and used for isobaric interference correction of ^{54}Cr on ^{54}Fe and ^{58}Ni on ^{58}Fe with a ^{54}Cr/^{53}Cr ratio of 0.2489 and ^{60}Ni/^{58}Ni ratio of 0.3852, respectively (Meija *et al.* 2016, de Vega *et al.* 2020). The details of the *in situ* Fe isotopic measurement method are described by Feng *et al.* (2022). We used the new isotopic reference material IRMM-524A (de Vega *et al.* 2020) as the "external" reference material to replace the international reference material IRMM-014 because the latter is nearly exhausted and not readily available. IRMM-524A iron metal has the same value as IRMM-014 within experimental uncertainty and has been proven to be feasible for *in situ* Fe isotope measurement (Xu *et al.* 2022). Meanwhile, PAS-Py600, PAS-Cpy400 (Feng *et al.* 2022) and Aa018 (Chen *et al.* 2021a) were used as unknown samples to verify the data quality. The Fe isotopic composition was expressed in delta (δ) notation (per mill, ‰) as follows:

$$\delta^{x}\mathrm{Fe} = \left[\left({}^{x}\mathrm{Fe}/{}^{54}\mathrm{Fe}\right)_{\mathrm{sample}}/\left({}^{x}\mathrm{Fe}/{}^{54}\mathrm{Fe}\right)_{\mathrm{RM}}\right]-1 \quad (2)$$

where "sample" and "RM" represent the measured samples and the reference material IRMM-524A, respectively, and x is mass number 56 or 57. All of the measurement results were converted to the reference value of IRMM-014.

For Cu isotope measurement, ion beams of ^{63}Cu and ^{65}Cu were collected in L2 and C Faraday cups, respectively. The mass spectrometer was operated in the low mass resolution mode with a resolving power of approximately 400 (peak edge width from 5% to 95% of the full peak height). Individual data acquisition consisted of one block of 120 cycles and an integration time of 0.524 s per cycle. The reference material JGZ-78 (Yang *et al.* 2023) was employed as the calibration material, whereas chalcopyrite TC1725 (Bao *et al.* 2021a) and JGZ-29 (Yang *et al.* 2023) were analysed as unknown samples to correct instrument time drift and verify the data quality. The detail of reference materials JGZ-29, JGZ-78 and TC1725 are listed in Table 3.

The final Cu isotopic composition was expressed in delta (δ) notation (per mill, ‰) as follows:

$$\delta^{65}\mathrm{Cu} = \left[\left({}^{65}\mathrm{Cu}/{}^{63}\mathrm{Cu}\right)_{\mathrm{sample}}/\left({}^{65}\mathrm{Cu}/{}^{63}\mathrm{Cu}\right)_{\mathrm{RM}}\right]-1 \quad (3)$$

where "sample" and "RM" represent the measured samples and the reference material JGZ-78, respectively. All δ values were converted to NIST SRM 976 for inter-laboratory comparisons. All of the *in situ* measurement data in this study were processed using the Iso-compass software (Zhang *et al.* 2020).

Bulk Fe-Cu isotope measurements by SN-MC-ICP-MS

SN-MC-ICP-MS for Fe and Cu isotope measurements was performed at the GPMR and Wuhan Sample Solution Analytical Technology Co. Ltd., respectively. For Fe isotope measurements, sample powders (~ 200 mg) were dissolved in a HF–HNO$_3$–HCl (+0.001% H$_2$O$_2$) system. Iron purification was performed according to the method described by Huang *et al.* (2011). Matrix elements were removed from the AG-MP-1M resin column in 9 ml of 8 mol l^{-1} HCl, while Fe was collected using 15 ml of 0.5 mol l^{-1} HCl and 1 ml of high-purity water. The same column procedure was repeated twice to ensure complete elimination of the matrices. The final Fe eluate was dried, and its condition was converted in 0.35 mol l^{-1} HNO$_3$ for isotopic measurement. The total procedural blank of Fe was approximately 20 ng, which was considered negligible for analysis. Geological reference materials BCR-2, BHVO-2 and GSB, were analysed as quality control reference materials. Details of the solution Fe isotopic measurements have been described by Lei *et al.* (2022).

For Cu isotope measurement, approximately 10–30 mg of the sample powders were dissolved using the HF and HNO$_3$ procedure. After complete digestion, 1 ml of HCl was added, and the mixture was evaporated to dryness. For chemical purification, the chromatographic procedure was modified according to the methods described by Maréchal *et al.* (1999) and Liu *et al.* (2014). The residue in these samples was dissolved in 1 ml of 8 mol l^{-1} HCl + 0.001% H$_2$O$_2$. A 1 ml sample solution was loaded onto 2 ml pre-cleaned AG-MP-1M resin. After elution of the matrix elements with 9 ml 8 mol l^{-1} HCl + 0.001% H$_2$O$_2$, 28 ml 8 mol l^{-1} HCl + 0.001% H$_2$O$_2$ was used to collect Cu. The final Cu elution solution was evaporated to dryness and converted to nitrate by re-addition and re-evaporation of 0.5 ml purified HNO$_3$ and 0.5 ml high-purity (Milli-Q™) water twice, separately. Finally, these samples were redissolved in 2% HNO$_3$ for isotopic measurement. All Cu isotope data were measured relative to NIST SRM 3114 and then converted to NIST SRM 976 after $\delta^{65}\mathrm{Cu}_{\mathrm{NIST\ SRM\ 976}} = \delta^{65}\mathrm{Cu}_{\mathrm{sam\text{-}NIST\ SRM\ 3114}} + 0.18$ calculation (Hou *et al.* 2016). The details of the solution Cu isotopic measurements are described by Zhu *et al.* (2019).

Bulk S isotope measurements by IRMS

Randomly selected pure minerals of LI-Cpy, LI-Po and LI-Sp in different sub-package tubes were milled into powders for bulk sulfur isotope determinations. The LI-Cpy and LI-Po experiments were conducted at the Beijing Research Institute of Uranium Geology (BRIUG), Beijing Createch Testing Technology, Co., Ltd (BCTT), the Chengdu University of Technology (CDUT), Institute of Geochemistry, Chinese Academy of Sciences (IGCAS), Laboratory for Stable Isotope Geochemistry, Institute of Geology and Geophysics (LSIGIGG), and the State Key Laboratory of Biogeology and Environmental Geology (BGEG) and the Nanjing Institute of Geology and Palaeontology, CAS (NIGPCAS). The Ll-Sp minerals were analysed at IGCAS, BRIUG and BGEG.

For the BRIUG and LSIGIGG analytical procedures, approximately 8 mg of sulfide powder were individually mixed with Cu_2O and further milled in an agate mortar. These mixtures were then reacted under vacuum at 980 °C, and the produced SO_2 gas was measured by a MAT-251 or Delta-S (Thermo Fisher Scientific Inc) mass spectrometer using the standard dual-inlet protocol (Chen *et al.* 2021b).

For the analytical procedures of IGCAS, BCTT and NIGPCAS, experiments were performed using a MAT-253 mass spectrometer (Thermo Finnigan, USA) combined with a Flash EA 2000 element analyser and a continuous flow (Conflo IV) unit. Approximately 100 μg of sulfide samples were packed into a tin capsule and delivered into a reactor, which was filled with oxidant tungsten trioxide (WO_3) and the reducing agent elemental Cu. When the sample fell into the reaction tube, oxygen was injected into the reactor. The sample and tin capsules were flash-combusted to produce SO_2 and SO_3 gases. Finally, the gas was carried into the mass spectrometer by helium. The precision values of repeated analysis of IAEA S1 (-0.3‰), IAEA S2 (+22.62‰) and IAEA S3 (-32.49‰) were better than 0.2‰ (1*s*) (Baublys *et al.* 2004).

For the analytical procedures at BGEG and CDUT, the sulfide powder and the reference materials were individually weighed into tin capsules and mixed with oxidation catalyst V_2O_5. The capsules were then flash-combusted at 1050 °C in a single quartz tube filled with high-purity oxidising (tungsten trioxide, WO_3) and reducing (elemental Cu) agents. The combustion-derived gases SO_2 were measured using EA-IRMS (Thermo Fisher Scientific Delta V Plus) after separation and purification (Feng *et al.* 2018).

Results and discussion

Chemical compositions of sulfide samples

EPMA and LA-ICP-MS were used to measure the chemical compositions of the candidate reference materials, and the results are listed in Tables 5 and S1 (Appendix S2). Measurement results from EPMA show that Ll-Cpy fragments (n = 15) are relatively homogeneous in chemical compositions with the mass fraction of Fe ranging from 30.42% *m/m* to 30.85% *m/m*, Cu ranging from 33.28% *m/m* to 33.71% *m/m*, and the S ranging from 35.54% *m/m* to 35.937% *m/m*. The mass fractions of Fe and S in Ll-Po fragments (n = 20) range from 60.11% *m/m* to 60.77% *m/m* and from 9.27% *m/m* to 39.83% *m/m*, respectively. In the fifteen individual grains analyses of Ll-Sp sample, the mass fraction of Fe ranges from 7.27% *m/m* to 8.01% *m/m*, Zn ranges from 58.45% m/m to 59.44% *m/m*, and the S ranges from 32.80% *m/m* to 33.22% *m/m*. EPMA measurements reveal homogeneous major element compositions in the candidate chalcopyrite, pyrrhotite and sphalerite samples.

Forty-five fragments of Ll-Cpy and Ll-Po were randomly selected for element mass fraction determination by LA-ICP-MS. NIST SRM 610 (Jochum *et al.* 2005) was used for instrument time-drift correction, while sulfide reference material MASS-1 (Wilson *et al.* 2002) was used for calibration and Fe was used as the internal standard element for the quantitative calibration. The measurement results are presented in Table S1 (Appendix S2). The Cr mass fraction in Ll-Cpy and Ll-Po are 0.66 ± 30 μg g^{-1} (1*s*, k = 45) and 1.22 ± 0.24 μg g^{-1} (1*s*, k = 45), whereas the Cr/Fe (the content ratio of elements Cr and Fe) in Ll-Cpy and Ll-Po are 2.15×10^{-6} and 2.02×10^{-6}, respectively. According to the research results of Lei *et al.* (2022), when Cr/Fe in the sample is less than 1.00×10^{-4}, no detectable deviation in Fe isotope ratio will be observed. Despite the heterogeneous distribution of certain trace elements, they do not affect the determination of the S-Fe-Cu isotopes.

The backscattered electron (BSE) images of random fragments in the Ll-Cpy, Ll-Po and Ll-Sp epoxy resin mounts are shown in Figure 3. Most sulfide fragments (Figure 3a) show a clean sample surface; however, a few silicate inclusions may be present in certain fragments. The inclusions' characteristics were easily identified and avoided during *in situ* analysis. Overall, the flat and clean surfaces of the candidate sulfide samples make them suitable for microanalysis.

Homogeneity assessment of sulfur isotopes in Ll-Cpy, Ll-Po and Ll-Sp

At the GPMR, fs-LA-MC-ICP-MS S isotope measurements were conducted for two years for assessment of long-term stability and homogeneity (Figures 4–6); each random fragment in different epoxy resin mounts was analysed using

Table 5.
EPMA measurement results for element mass fractions (g 100 g^{-1}) in chalcopyrite Ll-Cpy, pyrrhotite Ll-Po and sphalerite Ll-Sp

Sample	No.	Ni	Mn	As	Fe	Cu	Zn	S	Total
Ll-Cpy	Spot 1	0.00	0.02	0.00	30.51	33.28	0.05	35.54	99.39
	Spot 2	0.00	0.00	0.01	30.53	33.52	0.06	35.68	99.80
	Spot 3	0.00	0.00	0.00	30.64	33.32	0.06	35.48	99.51
	Spot 4	0.00	0.01	0.00	30.85	33.47	0.06	35.60	99.99
	Spot 5	0.00	0.01	0.00	30.53	33.47	0.05	35.68	99.74
	Spot 6	0.00	0.01	0.01	30.62	33.71	0.04	35.57	99.96
	Spot 7	0.01	0.00	0.00	30.58	33.42	0.08	35.70	99.79
	Spot 8	0.00	0.00	0.00	30.61	33.46	0.04	35.59	99.70
	Spot 9	0.00	0.00	0.01	30.70	33.36	0.05	35.70	99.83
	Spot 10	0.00	0.00	0.00	30.77	33.30	0.05	35.75	99.87
	Spot 11	0.00	0.00	0.00	30.73	33.54	0.03	35.91	100.21
	Spot 12	0.00	0.01	0.00	30.73	33.37	0.07	35.73	99.92
	Spot 13	0.00	0.01	0.00	30.74	33.39	0.06	35.77	99.96
	Spot 14	0.00	0.00	0.02	30.42	33.64	0.04	35.85	99.97
	Spot 15	0.00	0.00	0.00	30.77	33.41	0.04	35.93	100.15
	Mean val.	**0.00**	**0.00**	**0.00**	**30.65**	**33.45**	**0.05**	**35.70**	**99.85**
Ll-Po	Spot 1	0.00	0.00	0.00	60.34	0.03	0.00	39.71	100.08
	Spot 2	0.00	0.02	0.00	60.40	0.03	0.03	39.44	99.91
	Spot 3	0.01	0.00	0.00	60.26	0.02	0.00	39.44	99.73
	Spot 4	0.01	0.01	0.00	60.67	0.01	0.00	39.57	100.28
	Spot 5	0.00	0.01	0.01	60.16	0.03	0.01	39.59	99.80
	Spot 6	0.01	0.00	0.00	60.43	0.03	0.00	39.40	99.87
	Spot 7	0.00	0.00	0.00	60.55	0.02	0.02	39.47	100.08
	Spot 8	0.00	0.01	0.00	60.77	0.01	0.01	39.44	100.25
	Spot 9	0.00	0.00	0.00	60.15	0.05	0.00	39.62	99.82
	Spot 10	0.00	0.00	0.02	60.17	0.02	0.00	39.56	99.77
	Spot 11	0.00	0.00	0.00	60.20	0.03	0.00	39.70	99.93
	Spot 12	0.00	0.00	0.01	60.19	0.04	0.02	39.49	99.75
	Spot 13	0.00	0.00	0.01	60.18	0.04	0.00	39.27	99.49
	Spot 14	0.00	0.00	0.01	60.26	0.03	0.01	39.66	99.97
	Spot 15	0.00	0.00	0.00	60.15	0.02	0.00	39.64	99.80
	Spot 16	0.00	0.00	0.02	60.15	0.05	0.01	39.69	99.93
	Spot 17	0.01	0.01	0.00	60.11	0.05	0.00	39.79	99.96
	Spot 18	0.00	0.01	0.00	60.56	0.01	0.00	39.45	100.03
	Spot 19	0.00	0.00	0.00	60.46	0.00	0.00	39.45	99.92
	Spot 20	0.00	0.00	0.00	60.52	0.03	0.02	39.83	100.40
	Mean val.	**0.00**	**0.00**	**0.00**	**60.32**	**0.03**	**0.01**	**39.56**	**99.93**
Ll-Sp	Spot 1	0.00	0.15	0.00	7.74	0.00	58.63	33.04	99.57
	Spot 2	0.00	0.14	0.00	7.66	0.00	59.25	32.80	99.85
	Spot 3	0.01	0.16	0.02	7.89	0.00	58.63	33.04	99.74
	Spot 4	0.01	0.17	0.00	7.90	0.00	58.75	33.19	100.03
	Spot 5	0.00	0.17	0.01	7.89	0.00	58.74	32.98	99.78
	Spot 6	0.00	0.14	0.00	7.85	0.00	58.63	33.15	99.77
	Spot 7	0.00	0.12	0.01	7.41	0.00	59.36	32.93	99.84
	Spot 8	0.00	0.14	0.00	7.75	0.00	59.44	33.13	100.46
	Spot 9	0.03	0.15	0.00	7.85	0.00	58.94	32.92	99.89
	Spot 10	0.02	0.12	0.00	7.65	0.00	59.18	33.00	99.96
	Spot 11	0.00	0.15	0.00	8.01	0.00	58.45	32.97	99.58
	Spot 12	0.00	0.14	0.00	7.92	0.00	59.11	32.95	100.12
	Spot 13	0.02	0.15	0.00	8.01	0.00	58.66	33.22	100.07
	Spot 14	0.00	0.13	0.00	7.27	0.00	59.42	33.09	99.90
	Spot 15	0.00	0.15	0.00	7.83	0.00	58.79	32.96	99.73
	Mean val.	**0.01**	**0.15**	**0.00**	**7.77**	**0.00**	**58.93**	**33.03**	**99.89**

two to three spots. The measurement results for quality control reference materials PPP-1, HTS4-6 and SPH-1 are presented in Table S1 (Appendix S1).

Figure 4a, b show the results of Ll-Cpy (approximately 380 fragments) in different analysis period. In session 1 of Ll-Cpy (Figure 4a), the selected grains yielded mean $\delta^{34}S_{V\text{-}CDT}$

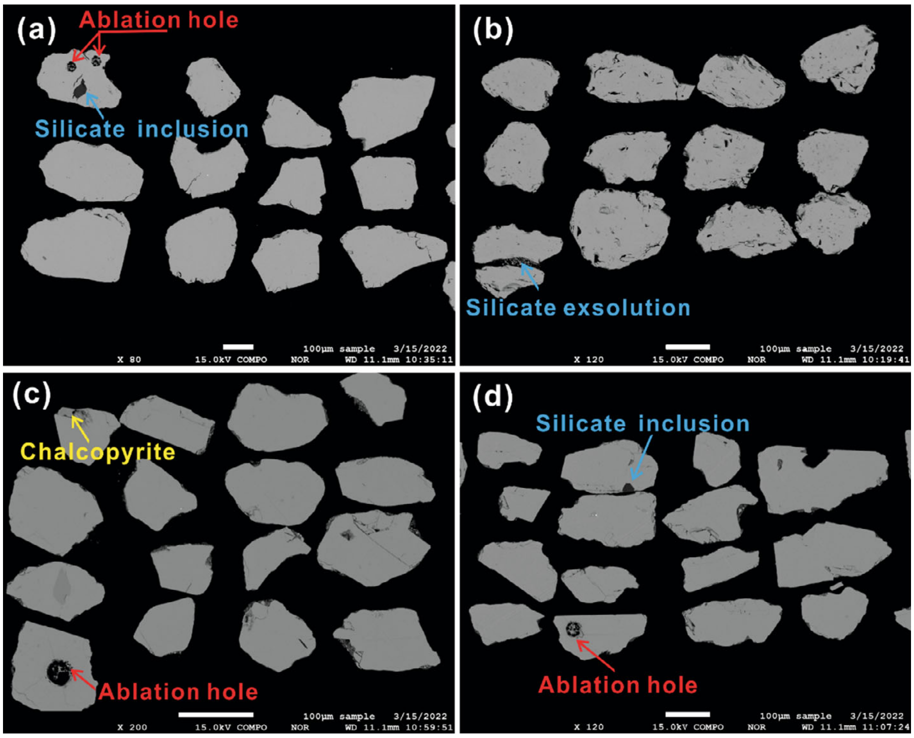

Figure 3. Backscattered electron images (BSE) of a random fragment in the (a) Ll-Cpy, (b) Ll-Po and (c–d) Ll-Sp epoxy resin mounts.

values of 6.19 ± 0.28‰ (2*s*, *n* = 488), while the mean $\delta^{34}S_{\text{V-CDT}}$ value was 6.23 ± 0.31‰ (2*s*, *n* = 274) in session 2 (Figure 4b). Sulfur isotopic compositions in different periods were identical with the external precision (2*s*) ranging from 0.28‰ to 0.31‰. All the results show normal distributions in the probability density plots (Figure 4c, d), indicating the excellent sulfur isotopic homogeneity of the chalcopyrite Ll-Cpy. The *in situ* S isotope measurement results for Ll-Cpy in different measurement sessions are presented in Table S2 (Appendix S2).

Figure 5a, b shows the sulfur isotopic composition of Ll-Po (approximately 110 fragments) during the two analysis periods. In session 1 of Ll-Po (Figure 5a), the grains yielded a mean $\delta^{34}S_{\text{V-CDT}}$ value of 6.12 ± 0.36‰ (2*s*, *n* = 207), which is consistent with the value 6.28 ± 0.35‰ (2*s*, *n* = 129) of session 2 (Figure 5b) within the uncertainty. Meanwhile, there no abnormal data were found in the probability density plots (Figure 5c, d), indicating good sulfur isotopic homogeneity of pyrrhotite Ll-Po. The *in situ* S isotope results of Ll-Po in different measurement sessions are presented in Table S3 (Appendix S2).

For the Ll-Sp, the $\delta^{34}S_{\text{V-CDT}}$ values of session 1 (Figure 6a) and 2 (Figure 6b) are 6.29 ± 0.38‰ (2*s*, *n* = 107) and 6.19 ± 0.37‰ (2*s*, *n* = 361), respectively. Repeated analyses of the Ll-Sp samples in approximately 230 fragments yielded a good external reproducibility of 0.37‰, which not only indicated the homogeneous distribution of sulfur isotopes but also met the requirement of *in situ* sulfur isotope measurement by fs-LA-MC-ICP-MS (Figure 6c, d). The *in situ* S isotope results of Ll-Sp in different measurement sessions are presented in Table S4 (Appendix S2).

Meanwhile, the *in situ* sulfur isotope ratios of Ll-Cpy and Ll-Po were determined using ns-LA-MC-ICP-MS at the SKLCD (Table S5, Appendix S2). The measurement results for the quality control reference materials TC1725 and RPPY are listed in Table S2 (Appendix S1). The mean values of Ll-Cpy and Ll-Po obtained at the SKLCD are 6.29 ± 0.34‰ (2*s*, *n* = 15) and 6.14 ± 0.28‰ (2*s*, *n* = 18), respectively. These values are consistent with the results obtained at the GPMR (Table 6). All of the *in situ* measurement results for the candidate chalcopyrite, pyrrhotite and sphalerite samples showed extremely homogenous in sulfur isotope ratios.

Randomly selected Ll-Cpy, Ll-Po and Ll-Sp grains in different sub-package tubes (Figure 2) were analysed using bulk analytical methods in different laboratories to assess the S isotope composition (Figure 7 and Table S6 in Appendix S2). The measurement results of the reference materials by IRMS are listed in Table S2 (Appendix S1). All

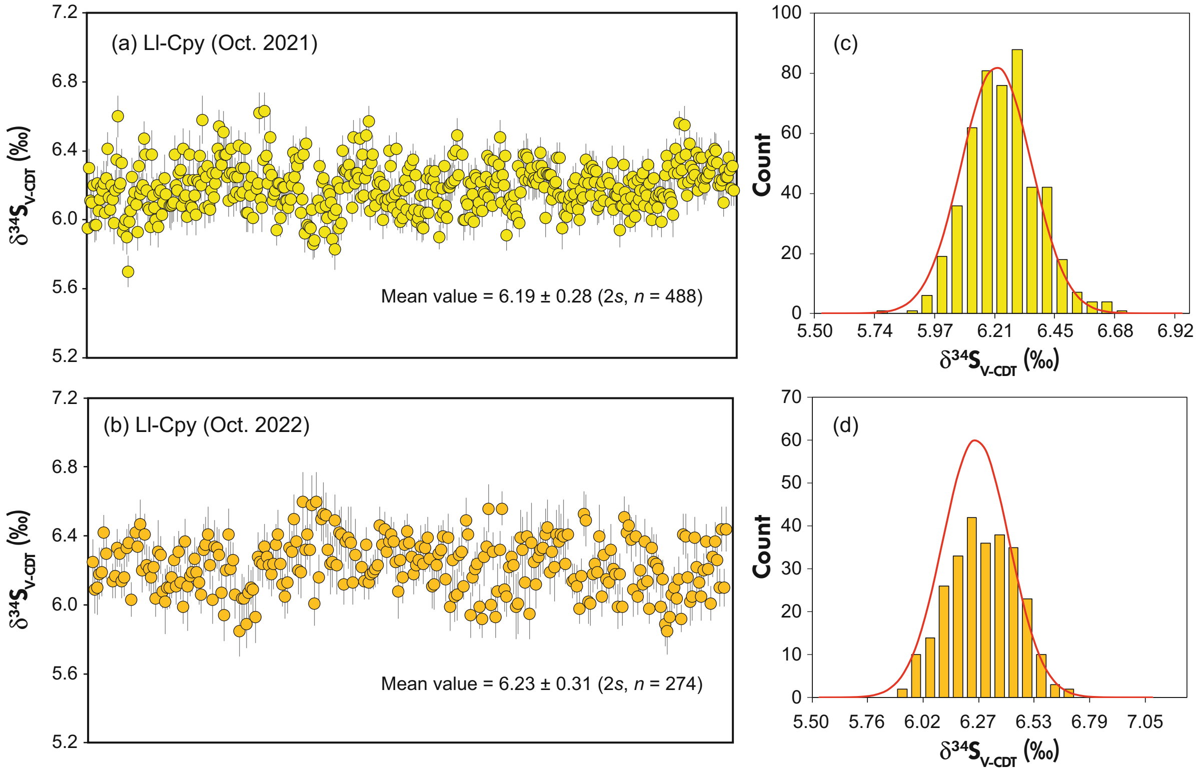

Figure 4. Plots of fs-LA-MC-ICP-MS measurement results for Ll-Cpy in different analysis periods. Sulfur isotope measurement results in (a) session 1 and (b) session 2. (c) and (d) show the histograms of $\delta^{34}S_{V\text{-}CDT}$ values in (a) and (b), respectively. The range bars for single analyses represent 2SE.

$\delta^{34}S_{V\text{-}CDT}$ values obtained by independently IRMS laboratories are consistent within analytical uncertainty, and the mean bulk analysis values agree well with the LA-MC-ICP-MS results (Table 6). Considering the isotope ratio uncertainty contributed from the uncertainties of bracketing calibrator and normalisation materials, we combined the experimental standard deviation, the reproducibility of the reference materials, and the uncertainty of the reference values of the reference materials into the final data. The final recommended $\delta^{34}S_{V\text{-}CDT}$ values for Ll-Cpy, Ll-Po and Ll-Sp are 6.13 ± 0.37‰ (2*s*), 6.42 ± 0.37‰ (2*s*) and 6.28 ± 0.38‰ (2*s*), respectively (Figure 7 and Table S3 in Appendix S1).

Homogeneity assessment of the iron isotope in Ll-Cpy and Ll-Po

In this study, we performed Fe isotope homogeneity assessment experiments on Fe-bearing chalcopyrite Ll-Cpy and pyrrhotite Ll-Po (Figure 8). Approximately sixty-four and fifty-nine individual fragments in the Ll-Cpy and Ll-Po mounts, respectively, were selected for LA-MC-ICP-MS Fe isotope composition analyses and the mean $\delta^{56}Fe_{IRMM\text{-}014}$ values for Ll-Cpy and Ll-Po are 0.60 ± 0.17‰ (2*s*, *n* = 64) and -0.67 ± 0.18‰ (2*s*, *n* = 59), respectively. We combined the experimental standard deviation, the reproducibility of the reference materials, and the uncertainty of the reference values of the reference materials into the final SN-MC-ICP-MS results. The recommended $\delta^{56}Fe_{IRMM\text{-}014}$ values for Ll-Cpy and Ll-Po are 0.60 ± 0.07‰ (2*s*) and 6.39 ± 0.37‰ (2*s*), respectively (Figure 8 and Table S3 in Appendix S1). The results demonstrated that the Fe isotope composition in Ll-Cpy and Ll-Po samples were homogeneous and could be used as potential reference materials for sulfide Fe isotope measurement. The detailed Fe isotopic compositions of Ll-Cpy and Ll-Po, obtained using LA/SN-MC-ICP-MS, are listed in Table S7 (Appendix S2). The measurement results of the quality control reference materials during *in situ* and bulk analyses are listed in Tables S4 and S5 (Appendix S1).

Homogeneity assessment of the copper isotope in Ll-Cpy

The Cu isotopic characteristics of the Cu-bearing chalcopyrite Ll-Cpy reference material were analysed using fs-LA-MC-ICP-MS (Figure 9). A total of 164 fragments in different Ll-Cpy mounts were randomly selected for *in situ* Cu

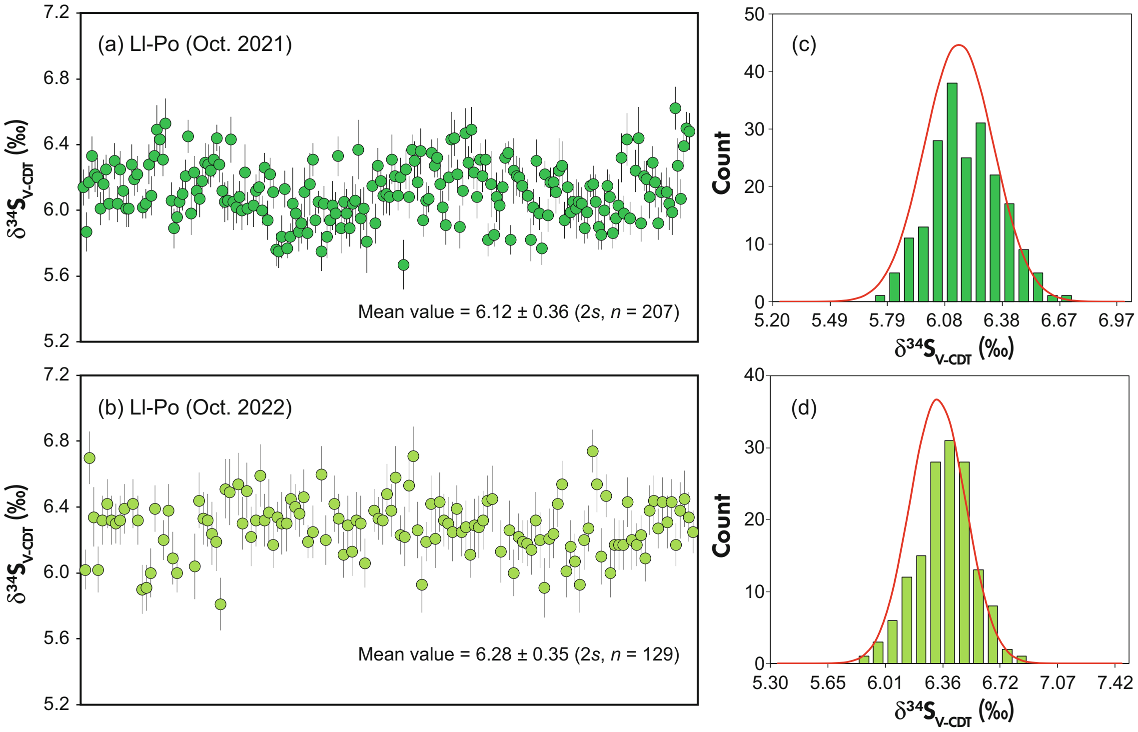

Figure 5. Plots of fs-LA-MC-ICP-MS measurement results for Ll-Po in different analysis periods. Sulfur isotope measurement results in (a) session 1 and (b) in session 2. (c) and (d) are the histograms of $\delta^{34}S_{V\text{-}CDT}$ values in (a) and (b), respectively. The range bars for single analyses represent 2SE.

isotope measurement, and the obtained LA value of 0.58 ± 0.15‰ (2*s*, *n* = 164) coincided with the value 0.57 ± 0.06‰ (2*s*) obtained by solution analyses. The solution value also combined the experimental standard deviation, the reproducibility of the reference materials and the uncertainty of the reference values of the reference materials. Repeated analyses of the Ll-Cpy yielded a good "external reproducibility" of 0.15‰. The homogenous of Cu isotopic composition and good agreement between the laser and solution values indicate that the Ll-Cpy sample can be used as a reference material for *in situ* Cu isotope analysis. The Cu isotope composition of Ll-Cpy obtained by LA/SN-MC-ICP-MS is listed in Table S8 (Appendix S2). The measurement results of the quality-control reference materials used during *in situ* and bulk analyses are listed in Tables S6 and S7 (Appendix S1).

Analytical feasibility of the new reference materials

Ll-Cpy, Ll-Po and Ll-Sp were used as bracketing calibrators to determine the S-Fe-Cu isotopic ratios of the reported sulfide reference materials with well-known isotopic compositions (Figure 10). The abscissa represents the reference values of the reported sulfide reference materials, whereas the measured values obtained in this study are shown on the ordinate. The $\delta^{34}S_{V\text{-}CDT}$ results for pyrite PPP-1, pentlandite JC-Pn, pyrrhotite JC-Po, chalcopyrite TC1725, synthesised pyrite PAS-Py600 and synthesised chalcopyrite PAS-Cpy400 were 5.44 ± 0.14‰ (2*s*, *n* = 7), -0.14 ± 0.16‰ (2*s*, *n* = 7), 0.17 ± 0.18‰ (2*s*, *n* = 7), 12.35 ± 0.20‰ (2*s*, *n* = 7), 18.44 ± 0.13‰ (2*s*, *n* = 7) and 10.55 ± 0.17‰ (2*s*, *n* = 7), respectively. The measured $\delta^{56}Fe_{IRMM\text{-}014}$ results of JC-Pn, JC-Po, PAS-Py600 and PAS-Cpy400 are 1.41 ± 0.15‰ (2*s*, *n* = 4), -0.46 ± 0.22‰ (2*s*, *n* = 4), 0.21 ± 0.09‰ (2*s*, *n* = 4) and 0.01 ± 0.09‰ (2*s*, *n* = 4), respectively. The Cu isotope results of PAS-Cpy400 and TC1725 are 0.36 ± 0.10‰ (2*s*, *n* = 4) and -0.01 ± 0.13‰ (2*s*, *n* = 4), respectively. All the measurement results (Table S9, Appendix S2) were in good agreement with the reference values, plotting close to the 1:1 lines in Figure 10 (a–d). Therefore, we conclude that Ll-Cpy, Ll-Po and Ll-Sp are ideal calibration and quality control reference materials for *in situ* S-Fe-Cu isotope measurements.

Conclusions

In this study a set of potential reference materials, Ll-Cpy (chalcopyrite), Ll-Po (pyrrhotite) and Ll-Sp (sphalerite),

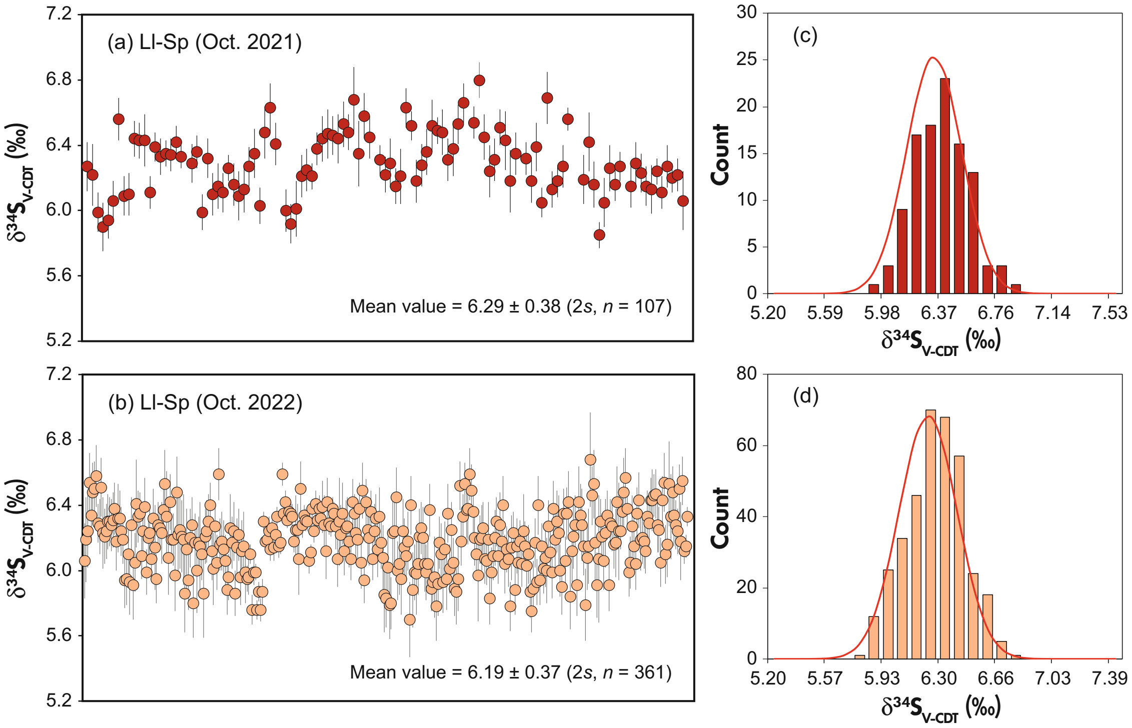

Figure 6. Plots of fs-LA-MC-ICP-MS measurement results for Ll-Sp in different analyses period. Sulfur isotope measurement results in (a) session 1 and (b) in session 2. (c) and (d) are the histograms of $\delta^{34}S_{V\text{-}CDT}$ values in (a) and (b), respectively. The range bars for single analyses represent 2SE.

Table 6.
Summary of mean values of sulfur isotopes ($\delta^{34}S$) from bulk and *in situ* methods, and recommended values in chalcopyrite Ll-Cpy, pyrrhotite Ll-Po and sphalerite Ll-Sp

Method	Laboratory	Ll-Cpy			Ll-Po			Ll-Sp		
		$\delta^{34}S$ (‰)	2*s*	*n*	$\delta^{34}S$ (‰)	2*s*	*n*	$\delta^{34}S$ (‰)	2*s*	*n*
IRMS	BRIUG	6.19	0.06	12	6.23	0.09	12	6.24	0.15	12
	BGEG	6.14	0.19	9	6.27	0.23	7	6.19	0.24	5
	IGCAS	5.92	0.13	4	6.35	0.11	4	6.41	0.06	4
	CDUT	5.98	0.08	4	6.42	0.06	4	-	-	-
	BCTT	6.24	0.14	6	6.55	0.21	6	-	-	-
	NIGPCAS	6.43	0.15	6	6.66	0.17	6	-	-	-
	LSIGIGG	5.99	0.24	5	6.54	0.05	5	-	-	-
LA-MC-ICP-MS	GPMR session 1	6.19	0.28	488	6.12	0.36	207	6.29	0.28	117
	GPMR session 2	6.23	0.31	274	6.28	0.31	129	6.19	0.37	361
	SKLCD	6.29	0.34	15	6.14	0.28	18	-	-	-
Recommended value		6.13	0.37	-	6.42	0.37	-	6.28	0.38	-

The uncertainty of the recommended value is the combined uncertainty.

were developed for *in situ* S-Fe-Cu isotope measurements. The results obtained from bulk and *in situ* measurements indicate that Ll-Cpy, Ll-Po and Ll-Sp have homogeneous S-Fe-Cu isotopic compositions. The recommended $\delta^{34}S_{V\text{-}CDT}$ values for Ll-Cpy, Ll-Po and Ll-Sp are 6.13 ± 0.37‰ (2*s*), 6.42 ± 0.37‰ (2*s*) and 6.28 ± 0.38‰ (2*s*), respectively. The recommended $\delta^{56}Fe_{IRMM\text{-}014}$ values of Ll-Cpy and Ll-Po are 0.57 ± 0.07‰ (2*s*) and -0.62 ± 0.07‰ (2*s*), respectively. The determined mean $\delta^{65}Cu_{NIST\ SRM\ 976}$ in Ll-Cpy is 0.57 ± 0.06‰ (2*s*). These reference materials exist in sufficient quantity for sharing with other laboratories worldwide.

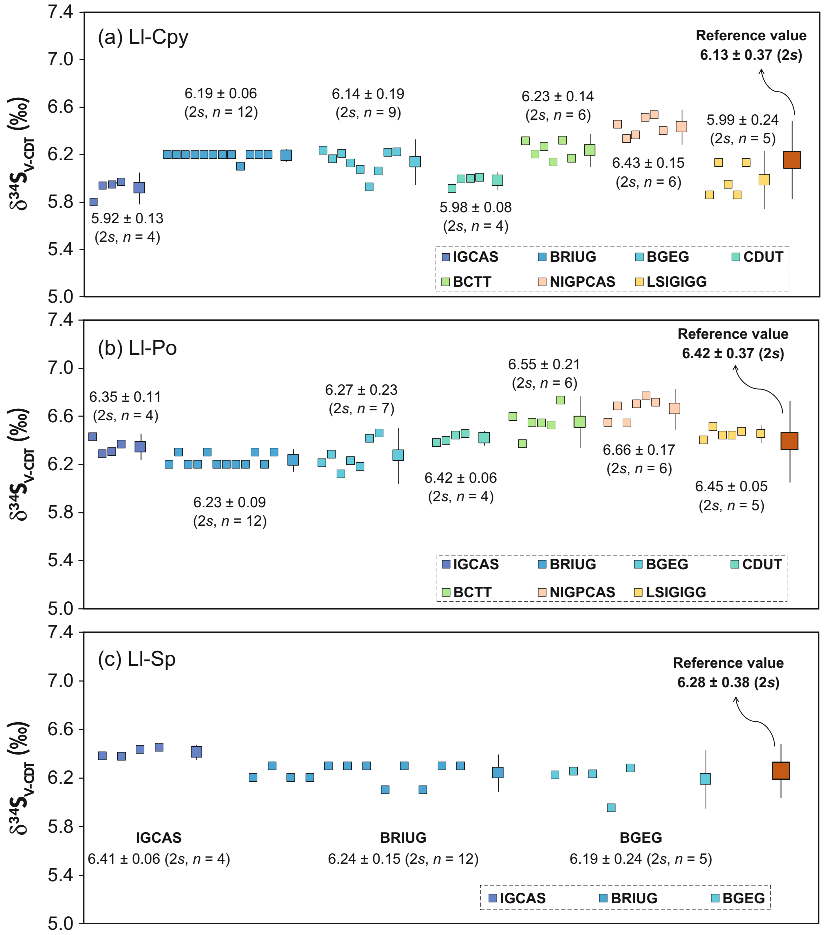

Figure 7. Plots of bulk sulfur isotope composition of (a) LI-Cpy, (b) LI-Po and (c) LI-Sp obtained in different laboratories. The range bar for individual laboratories represents 2SE, and that for the mean values represents 2*s*. The uncertainty of bulk analyses results in different laboratories are expressed as experimental standard deviation while the uncertainty of the recommended value is the combined uncertainty.

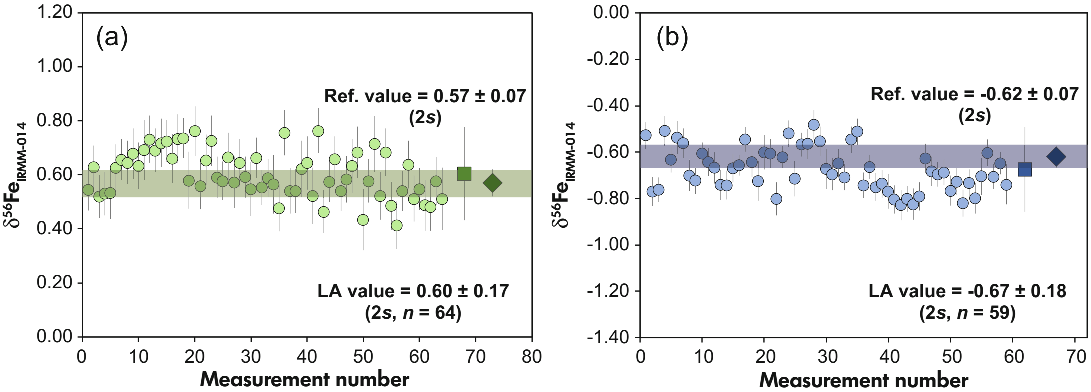

Figure 8. Plots of iron isotopic composition in (a) LI-Cpy and (b) LI-Po. The circles and squares represent random laser ablation spot results and the mean results, respectively, while the rhombuses are the bulk values determined by SN-MC-ICP-MS. The range bar for a single analysis represents 2SE, and that for the mean value represents 2*s*. The uncertainty of the recommended value is the combined uncertainty.

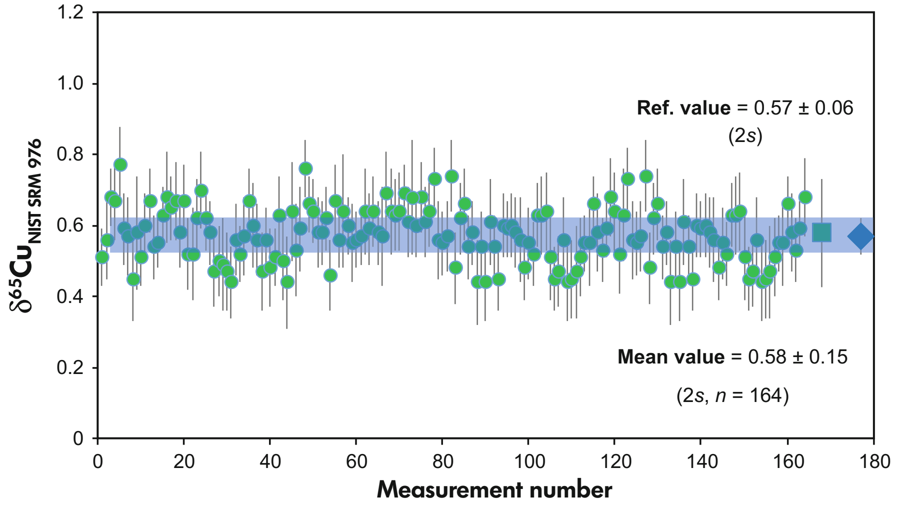

Figure 9. **Plot of copper isotopic composition in Ll-Cpy. The circles and squares represent random laser ablation spots results and the average results, respectively, while the rhombuses and bule shade are the bulk values analysed by SN-MC-ICP-MS. The range bar for a single analysis represents 2SE, and that for the mean value represents 2*s*. The uncertainty of the recommended value is the combined uncertainty.**

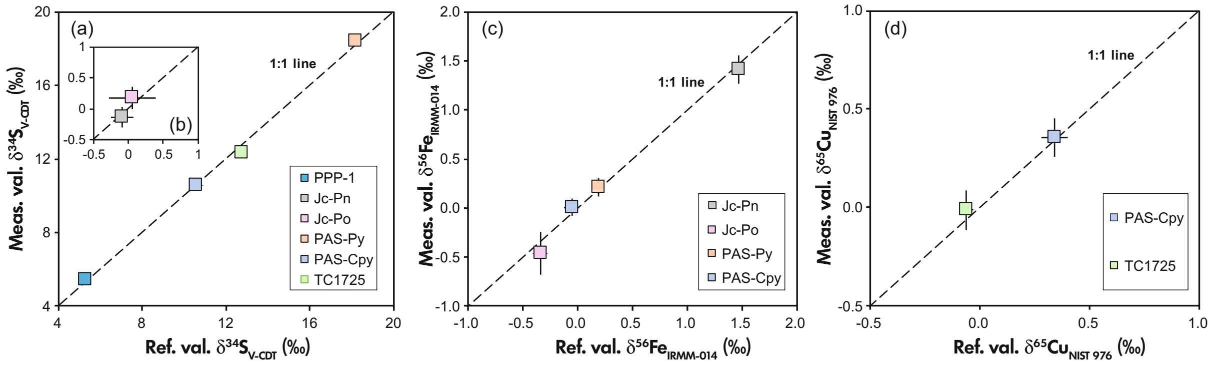

Figure 10. **Plots of measurement results for S (a, b), Fe (c) and Cu (d) isotopic compositions in different reference materials with Ll-Cpy, Ll-Po and Ll-Sp bracketing calibrators. The abscissa represents the reference values of reported sulfide reference materials, while the ordinate shows the measured value obtained in this study. Range bars represent 2*s*.**

Acknowledgements

This research was supported by the National Key R&D Program of China (2021YFC2903003), the National Natural Science Foundation of China (Grants 41973013, 41730211, 91962212 and 42272069), the Natural Science Foundation of Hubei Province (2020CFA045), the most special fund from the State Key Laboratory of Geological Processes and Mineral Resources, China University of Geosciences (MSFGPMR04 and MSFGPMR08), and the Second Tibetan Plateau Scientific Expedition and Research Program of China (2019QZKK0704).

We express thanks to Juan Han and Hanbin Liu from the Beijing Research Institute of Uranium Geology, Zihu Zhang from the State Key Laboratory of Biogeology and Environmental Geology, Jing Gu from the Institute of Geochemistry, Chinese Academy of Sciences, Xianguo Lang from the Chengdu University of Technology, Fengyong Xia from the Beijing Createch Testing Technology, Co., Ltd, Guocheng Guan from the Nanjing Institute of Geology and Palaeontology, Chinese Academy of Sciences, Hongwei Li from the Laboratory for Stable Isotope Geochemistry, Institute of Geology and Geophysics and Zhian Bao from the State Key Laboratory of Continental Dynamics (SKLCD), Northwest

University for the assistance in S isotope analyses. There are no conflicts of interest to declare. Scientific editing by Paul J. Sylvester.

Data availability statement

Data openly available in a public repository that issues datasets with DOIs.

References

Bao Z.A., Lv N., Chen K.Y., Luan Y., Sun X.H., Zong C.L. and Yuan H.L. (2021a)
A potential new chalcopyrite reference material for LA-MC-ICP-MS copper isotope ratio measurement. **Geostandards and Geoanalytical Research**, 45, 401–418.

Bao Z.A., Chen K.Y., Zong C.L. and Yuan H.L. (2021b)
TC1725: A proposed chalcopyrite reference material for LA-MC-ICP-MS sulfur isotope determination. **Journal of Analytical Atomic Spectrometry**, 36, 1657–1665.

Baublys K.A., Golding S.D., Young E. and Kamber B.S. (2004)
Simultaneous determination of $\delta^{33}S_{V\text{-}CDT}$ and $\delta^{34}S_{V\text{-}CDT}$ using masses 48, 49 and 50 on a continuous flow isotope ratio mass spectrometer. **Rapid Communications in Mass Spectrometry**, 18, 2765–2769.

Brzozowski M.J., Good D.J., Wu C.Z. and Li W.Q. (2021)
Iron isotope fractionation during sulfide liquid evolution in Cu-PGE mineralization of the eastern Gabbro, Coldwell Complex, Canada. **Chemical Geology**, 576, 1–17.

Chen K.Y., Yuan H.L., Bao Z.A. and Lv N. (2021a)
Accurate analysis of Fe isotopes in Fe-dominated minerals by excimer laser ablation MC-ICP-MS on wet plasma conditions. **Atomic Spectroscopy**, 42, 282–293.

Chen K.Y., Bao Z.A., Liang P., Nie X.J., Zong C.L. and Yuan H.L. (2022b)
Preparation of sulfur-bearing reference materials for *in situ* sulfur isotope measurements using laser ablation multicollector inductively coupled plasma-mass spectrometry. **Spectrochimica Acta Part B**, 188, 106344.

Chen L., Chen K.Y., Bao Z.A., Liang P., Sun T.T. and Yuan H.L. (2017)
Preparation of standards for *in situ* sulfur isotope measurement in sulfides using femtosecond laser ablation MC-ICP-MS. **Journal of Analytical Atomic Spectrometry**, 32, 107–116.

Chen L., Feng Y.T., Yu H.M., Zhang W., Kang J.T., Huang F., Hu Z.C. and Li X. H. (2022a)
Tianyu-Py pyrite: A new natural reference material for microbeam determination of iron isotopic ratios. **Journal of Analytical Atomic Spectrometry**, 37, 2300–2308.

Chen L., Liu Y., Li Y., Li Q.L. and Li X.H. (2021b)
New potential pyrrhotite and pentlandite reference materials for sulfur and iron isotope microanalysis. **Journal of Analytical Atomic Spectrometry**, 36, 1431–1440.

Chen L., Feng Y.T., Yu H.M., Li L., Ding X., Zhang W., Kang J.T. and Li X.H. (2023)
Mineralogical and geochemical characterization at a micro-scale of a new natural chalcopyrite reference material for *in-situ* Fe isotopic ratio analysis. **Atomic Spectroscopy**, 44, 14–23.

de Vega C.G., Chernonozhkin S.M., Grigoryan R., Costas-Rodriguez M. and Vanhaecke F. (2020)
Characterization of the new isotopic reference materials IRMM-524A and ERM-AE143 for Fe and Mg isotopic analysis of geological and biological samples. **Journal of Analytical Atomic Spectrometry**, 35, 2517–2529.

Fang Y., Yu H. M., Xie L.W., Fang S.B., Huang F. and Li W.Y. (2023)
A new potential natural chalcopyrite reference material for *in situ* copper isotope microanalysis. **Journal of Analytical Atomic Spectrometry**, https://doi.org/10.1039/d3ja00105a.

Feng Y.T., Zhang W., Hu Z.C., Liu Y.S., Chen K., Fu J.L., Xie J.Y. and Shi Q.H. (2018)
Development of sulfide reference materials for *in situ* platinum-group elements and S-Pb isotope analyses by LA-(MC)-ICP-MS. **Journal of Analytical Atomic Spectrometry**, 33, 2172–2183.

Feng Y.T., Zhang W., Hu Z.C., Luo T., Li M., Liu Y.S., Liu H. and Li Q.L. (2022)
A new synthesis scheme of pyrite and chalcopyrite reference materials for *in situ* iron and sulfur isotope analysis using LA-MC-ICP-MS. **Journal of Analytical Atomic Spectrometry**, 37, 551–562.

Fu J.L., Hu Z.C., Zhang W., Yang L., Liu Y.S., Li M., Zong K.Q., Gao S. and Hu S.H. (2016)
In situ sulfur isotopes ($\delta^{34}S$ and $\delta^{33}S$) analyses in sulfides and elemental sulfur using high sensitivity cones combined with the addition of nitrogen by laser ablation MC-ICP-MS. **Analytica Chimica Acta**, 911, 14–26.

Gilbert S.E., Danyushevsky L.V., Rodemann T., Shimizu N., Gurenko A., Meffre S., Thomas H., Large R.R. and Death D. (2014)
Optimisation of laser parameters for the analysis of sulphur isotopes in sulphide minerals by laser ablation ICP-MS. **Journal of Analytical Atomic Spectrometry**, 29, 1042–1051.

Hammerli J., Greber N.D., Martin L., Bouvier A.S., Kemp A.I.S., Fiorentini M.L., Spangenberg J.E., Ueno Y. and Schaltegger U. (2021)
Tracing sulfur sources in the crust via SIMS measurements of sulfur isotopes in apatite. **Chemical Geology**, 579, 120242.

Hiebert R.S., Bekker A., Houle M.G., Wing B.A. and Rouxel O.J. (2016)
Tracing sources of crustal contamination using multiple S and Fe isotopes in the Hart komatiite-associated Ni-Cu-PGE sulfide deposit, Abitibi greenstone belt, Ontario, Canada. **Mineralium Deposita**, 51, 919–935.

references

Hou Q.H., Zhou L., Gao S., Zhang T., Feng L.P. and Yang L. (2016)
Use of Ga for mass bias correction for the accurate determination of copper isotope ratio in the NIST SRM 3114 Cu standard and geological samples by MC-ICP-MS. Journal of Analytical Atomic Spectrometry, 31, 280–287.

Hu S.Y., Wang X.C., Tian L.Y., Martin L., Schoneveld L., Barnes S.J., Guagliardo P., Ding W.W. and Rickard W.D.A. (2022)
Variability of sulfur isotopes and trace metals in pyrites from the upper oceanic crust of the South China Sea basin, implications for sulfur and trace metal cycling in subsurface. Chemical Geology, 606, 120982.

Hu Z.C., Liu Y.S., Gao S., Xiao S.Q., Zhao. L.S., Günther D., Li M., Zhang W. and Zong K.Q. (2012)
A "wire" signal smoothing device for laser ablation inductively coupled plasma-mass spectrometry analysis. Spectrochimica Acta Part B, 78, 50–57.

Hu Z.C., Li X.H., Luo T., Zhang W., Crowley J., Li Q.L., Ling X.X., Yang C., Li Y., Feng L.P., Xia X.P., Zhang S.B., Wang Z.C., Guo J.L., Xu L., Lin J., Liu X.M., Bao Z.A., Liu Y.S., Zong K.Q., Chen W. and Hu S.H. (2021)
Tanz zircon megacrysts: A new zircon reference material for the microbeam determination of U-Pb ages and Zr-O isotopes. Journal of Analytical Atomic Spectrometry, 36, 2715–2734.

Huang F., Zhang Z. F., Lundstrom C. C. and Zhi X. C. (2011)
Iron and magnesium isotopic compositions of peridotite xenoliths from Eastern China. Geochimica et Cosmochimica Acta, 75, 3318–3334.

Jackson S.E. and Günther D. (2003)
The nature and sources of laser induced isotopic fractionation in laser ablation-multicollector-inductively coupled plasma-mass spectrometry. Journal of Analytical Atomic Spectrometry, 18, 205–212.

JCGM 100 (2008)
Evaluation of measurement data-guide to the expression of uncertainty in measurement. International Organization for Standardization (Geneva, Switzerland).

Jenner F.E. and Arevalo R.D. (2016)
Major and trace element analysis of natural and experimental igneous systems using LA-ICP-MS. Elements, 12, 311–316.

Jochum K.P., Nohl U., Herwig K., Lammel E., Stoll B. and Hofmann A.W. (2005)
GeoReM: A new geochemical database for reference materials and isotopic standards. Geostandards and Geoanalytical Research, 29, 333–338.

Ke L.L., Zhang H.Y., Liu J.J., Zhai D.G., Guo D.H., Yang J.K., Tan Q., Xu Y.W., Zhang M. and Wang S.G. (2017)
Fluid inclusion, H-O, S, Pb and noble gas isotope studies of the Aerhada Pb-Zn-Ag deposit, Inner Mongolia, NE China. Ore Geology Reviews, 88, 304–316.

LaFlamme C., Martin L., Jeon H., Reddy S.M., Selvaraja V., Caruso S., Bui T.H., Roberts M.P., Voute F., Hagemann S., Wacey D., Littman S., Wing B., Fiorentini M. and Kilburn M.R. (2016)
In situ multiple sulfur isotope analysis by SIMS of pyrite, chalcopyrite, pyrrhotite, and pentlandite to refine magmatic ore genetic models. Chemical Geology, 444, 1–15.

Lazarov M. and Horn I. (2015)
Matrix and energy effects during *in-situ* determination of Cu isotope ratios by ultraviolet-femtosecond laser ablation multicollector inductively coupled plasma-mass spectrometry. Spectrochimica Acta Part B, 111, 64–73.

Lehmann B., Pasava J., Sebek O., Andronikov A., Frei R., Xu L.G. and Mao J.W. (2022)
Early Cambrian highly metalliferous black shale in South China: Cu and Zn isotopes and a short review of other non-traditional stable isotopes. Mineralium Deposita, 57, 1167–1187.

Lei Y.T., Li M., Wang Z.C., Zhu Y.T., Hu Z.C., Li Y.S. and Chai X.N. (2022)
Iron isotopic measurement using large-geometry high-resolution multi-collector inductively coupled plasma-mass spectrometer. Atomic Spectroscopy, 43, 214–222.

Li R.C., Xia X.P., Chen H.Y. Wu N.P., Zhao T.P., Lai C.K., Yang Q. and Zhang Y.Q. (2020)
A potential new chalcopyrite reference material for secondary ion mass spectrometry sulfur isotope ratio analysis. Geostandards and Geoanalytical Research, 44, 485–500.

Li R.C., Xia X.P., Yang S.H, Chen H.Y. and Yang Q. (2018)
Off-mount calibration and one new potential pyrrhotite reference material for sulfur isotope measurement by secondary ion mass spectrometry. Geostandards and Geoanalytical Research, 43, 177–187.

Li W.Q., Jackson S.E., Norman J.P.V and Graham S. (2010)
Copper isotopic zonation in the Northparkes porphyry Cu-Au deposit, SE Australia. Geochimica et Cosmochimica Acta, 74, 4078–4096.

Liu S.A., Li D.D., Li S.G., Teng F.Z., Ke S., He Y.S. and Lu Y.H. (2014)
High-precision copper and iron isotope analysis of igneous rock standards by MC-ICP-MS. Journal of Analytical Atomic Spectrometry, 29, 122–133.

Luo T., Li Q.L., Ling X.X., Li Y., Yang C., Wang H.L., Xia X.P., Zhang S.B., Xu L., Liu X.M., Deng X.D. and Hu Z.C. (2021)
Jilin zircon – A new natural reference material for microbeam U-Pb geochronology and Hf-O isotopic analysis. Journal of Analytical Atomic Spectrometry, 36, 2216–2226.

Lv N., Bao Z.A., Chen K.Y., Zong C.L., Zhang Y. and Yuan H.L. (2022)
New potential sphalerite, chalcopyrite, galena and pyrite reference materials for sulfur isotope determination by laser ablation-MC-ICP-MS. Geostandards and Geoanalytical Research, 46, 451–463.

references

Marin-Carbonne J., Rollion-Bard C., Bekker A., Rouxel O., Agangi A., Cavalazzi B., Wohlgemuth-Ueberwasser C.C., Hofmann A. and McKeegan K.D. (2014)
Coupled Fe and S isotope variations in pyrite nodules from Archean shale. Earth and Planetary Science Letters, 392, 67–79.

Maréchal C.N., Télouk P. and Albarède F. (1999)
Precise analysis of copper and zinc isotopic compositions by plasma-source mass spectrometry. Chemical Geology, 156, 251–273.

McLoughlin N., Li M.H., Wacey D., Martin L.A.J., Shen Y.A. and Beukes N.J. (2023)
Microbial sulphur-cycling and atmospheric signatures in the 2.52 Ga Gamohaan Formation, South Africa. Earth and Planetary Science Letters, 602, 117941.

Meija J., Coplen T.B., Berglund M., Brand W. A., Bievre P.D, Groning M., Holden N.E., Irrgeher J., Loss R.D., Walczyk T. and Prohaska T. (2016)
Isotopic compositions of the elements 2013 (IUPAC Technical Report). Pure and Applied Chemistry, 88, 293–306.

Mount S.M., Potter E.G., Yang Z., Fayek M., Powell J.W., Chi G. and Rizo H.G. (2022)
Formation of the Triple R unconformity-related uranium deposit as revealed by Fe and S isotopes in pyrite. Geochemistry: Exploration, Environment, Analysis, 22, 1–25.

Müller W. and Fietzke J. (2016)
The role of LA-ICP-MS in palaeoclimate research. Elements, 12, 329–334.

Nasdala L., Corfu F., Schoene B., Tapster S.R., Wall C.J., Schmitz M.D., Ovtcharova M., Schaltegger U., Kennedy A.K., Kronz A., Reiners P.W., Yang Y.-H., Wu F. Y., Gain S.E.M., Griffin W.L., Szymanowski D., Chanmuang N C., Ende M., Valley J.W., Spicuzza M.J., Wanthanachaisaeng B. and Giester G. (2018)
GZ7 and GZ8-two zircon reference materials for SIMS U-Pb geochronology. Geostandards and Geoanalytical Research, 42, 431–457.

Oeser M., Dohmen R., Horn I., Schuth S. and Weyer S. (2015)
Processes and time scales of magmatic evolution as revealed by Fe-Mg chemical and isotopic zoning in natural olivines. Geochimica et Cosmochimica Acta, 154, 130–150.

Onuk P., Melcher F., Mertz-Kraus R., Gaebler H.-E. and Goldmann S. (2017)
Development of a matrix-matched sphalerite reference material (MUL-ZnS-1) for calibration of *in situ* trace element measurements by laser ablation-inductively coupled plasma-mass spectrometry. Geostandards and Geoanalytical Research, 41, 263–272.

Paiste K., Fike D.A., Kirsimae K., Jones C. and Lepland A. (2022)
Testing the global significance of the sulfur isotope record of the *ca.* 2.0 Ga Zaonega Formation: A micro-scale S isotope investigation. Geochimica et Cosmochimica Acta, 331, 86–104.

Resano M., Aramendía M., Rello L., Calvo M.L., Bérail S. and Pécheyran C. (2013)
Direct determination of Cu isotope ratios in dried urine spots by means of fs-LA-MC-ICP-MS. Potential to diagnose Wilson's disease. Journal of Analytical Atomic Spectrometry, 28, 98–106.

Sawaki Y., Tahata M., Komiya T., Hirata T., Han J. and Shu D. (2018)
Redox history of the Three Gorges region during the Ediacaran and Early Cambrian as indicated by the Fe isotope. Geoscience Frontiers, 9, 155–172.

Smith J.M., Ripley E.M., Li C.S. and Wasylenki L.E. (2022)
Cu and Ni isotope variations of country rock-hosted massive sulfides located near midcontinent rift intrusions. Economic Geology, 117, 195–211.

Sossi P.A., Halverson G.P., Nebel O. and Eggins S.M. (2015)
Combined separation of Cu, Fe and Zn from rock matrices and improved analytical protocols for stable isotope determination. Geostandards and Geoanalytical Research, 39, 129–149.

Wilson S.A., Ridley W.I. and Koenig A.E. (2002)
Development of sulfide calibration standards for the laser ablation inductively-coupled plasma-mass spectrometry technique. Journal of Analytical Atomic Spectrometry, 17, 406–409.

Wohlgemuth-Ueberwasser C.C. and Jochum K.P. (2015)
Capability of fs-LA-ICP-MS for sulfide analysis in comparison to ns-LA-ICP-MS: Reduction of laser induced matrix effects? Journal of Analytical Atomic Spectrometry, 30, 2469–2480.

Xu L., Yang J.H., Wang H., Xie L.W., Yang Y.H., Huang C. and Wu S.T. (2022)
Analytical feasibility of a new reference material (IRMM-524A Fe metal) for the *in situ* Fe isotopic analysis of pyrite and ilmenite without matrix effects by femtosecond LA-MC-ICP-MS. Journal of Analytical Atomic Spectrometry, 37, 1835–1845.

Yang W.W., Zhang W., Hu Z.C., Zhou L., Liu S.A., Qiu X.F. and Tong X.R. (2023)
Development of three chalcopyrites and one copper metal as potential reference materials for copper isotopic analysis by LA-MC-ICP-MS. Rapid Communications in Mass Spectrometry, 37, e9538.

Yu B., Zeng Q.D., Frimmel H.E., Zhou L.L., McClenaghan S.H., Drakou F., Wang Y.B., Chen P.W. and Yu C. (2021)
A magmatic-hydrothermal origin of the Xinfang gold deposit, Liaodong Peninsula, China, revealed by *in-situ* S-Pb isotopes and trace element analyses of pyrite. Resource Geology, 71, 144–160.

Zhang W., Hu Z.C., Feng L.P., Wang Z.C., Liu Y.S., Feng Y.T. and Liu H. (2022)
Accurate determination of Zr isotopic ratio in zircons by femtosecond laser ablation MC-ICP-MS with "wet" plasma technique. Journal of Earth Science, 33, 67–75.

references

Zhang W., Hu Z.C. and Liu Y.S. (2020)
Iso-Compass: New freeware software for isotopic data reduction of LA-MC-ICP-MS. **Journal of Analytical Atomic Spectrometry**, 35, 1087–1096.

Zhao Y., Liu S.A., Xue C.J. and Li M.L. (2022)
Copper isotope evidence for a Cu-rich mantle source of the world-class Jinchuan magmatic Ni-Cu deposit. **American Mineralogist**, 107, 673–683.

Zheng X.Y., Beard B.L., Lee S., Reddy T.R., Xu H. and Johnson C.M. (2017)
Contrasting particle size distributions and Fe isotope fractionations during nanosecond and femtosecond laser ablation of Fe minerals: Implications for LA-MC-ICP-MS analysis of stable isotopes. **Chemical Geology**, 450, 235–247.

Zheng X.Y., Beard B.L. and Johnson C.M. (2018)
Assessment of matrix effects associated with Fe isotope analysis using 266 nm femtosecond and 193 nm nanosecond laser ablation multi-collector inductively coupled plasma-mass spectrometry. **Journal of Analytical Atomic Spectrometry**, 33, 68–83.

Zhu Y.T., Li M., Wang Z.C., Zou Z.Q., Hu Z.C., Liu Y.S., Zhou L. and Chai X.N. (2019)
High-precision copper and zinc isotopic measurements in igneous rock standards using large-geometry MC-ICP-MS. **Atomic Spectroscopy**, 40, 206–214.

Supporting information

The following supporting information may be found in the online version of this article:

Appendix S1. Measurement results for "external" reference materials during the S-Fe-Cu isotope determinations (Tables S1–S7).

Appendix S2. S-Fe-Cu isotope ratio and feasibility analysis measurement results for the potential sulfide reference materials (Tables S1–S9).

This material is available from: http://onlinelibrary.wiley.com/doi/10.1111/ggr.12530/abstract (This link will take you to the article abstract).